 

# Size-Dependent Population of Trivalent Rare Earth Cations ($RE^{3+}$) in $[(RE)_2(H_2O)_2(SbW_9O_{33})(W_5O_{18})_2]^{15-}$, and Structural Characterization of a Luthetium–Polyoxotungstate Complex $[Lu_3(H_2O)_4(SbW_9O_{33})_2(W_5O_{18})_2]^{21-}$

**Haruo Naruke and Toshihiro Yamase***

Chemical Resources Laboratory, Tokyo Institute of Technology, 4259 Nagatsuta, Midori-ku, Yokohama 226-8503

(Received November 22, 2001)

The effect of ionic radius of trivalent rare earth cations ($RE^{3+}$) on the population at two square-antiprismatic sites (*Site I* and *Site II*) in $[(RE)_2(H_2O)_2(SbW_9O_{33})(W_5O_{18})_2]^{15-}$ was studied by luminescence spectroscopic and X-ray crystallographic measurements in the Eu/Y- and Eu/Lu-mixed systems. The results indicated that a small $RE^{3+}$ cation favorably occupies *Site II* where $RE^{3+}$ is coordinated by four bridging O atoms of $[SbW_9O_{33}]^{9-}$ and four terminal O atoms of $[W_5O_{18}]^{6-}$. With the help of a structural characterization of pure $[(RE)_2(H_2O)_2(SbW_9O_{33})(W_5O_{18})_2]^{15-}$ (RE = Er, Y, Dy, Eu, Sm), the large occupancy of small $RE^{3+}$ at *Site II* was explained by a favorable coordination of $[SbW_9O_{33}]^{9-}$ for small $RE^{3+}$. A trial of the isostructural Lu complex unexpectedly showed formation of a novel $[Lu_3(H_2O)_4(SbW_9O_{33})_2(W_5O_{18})_2]^{21-}$ complex which consists of two $[Lu(SbW_9O_{33})(W_5O_{18})]^{12-}$ groups linked by $[Lu(H_2O)_4]^{3+}$ with $C_2$ configuration.

Polyoxometalates bind rare earth ions ($RE^{3+/4+}$) to form coordination complexes, where the polyoxometalate groups can be regarded as O-donor ligands of $RE^{3+/4+}$. Structural and preparation chemistry of these complexes are of importance, because the $RE^{3+/4+}$ cations function as linkers among polyoxometalate groups for huge high-nuclearity clusters.[1–3] RE-containing polyoxometalates have also attracted much interest due to their photoluminescence properties[1,4–5] and catalytic activities.[6–8]

We recently reported a RE-polyoxotungstate complex, $[(RE)_2(H_2O)_2(SbW_9O_{33})(W_5O_{18})_2]^{15-}$ (Fig. 1), which comprises two different kinds (*Site I* and *Site II*) of square-antiprismatic sites for RE (Y, Sm, Eu, Dy, Er, and Ho).[9] *Site I* consists of two terminal O atoms from $[SbW_9O_{33}]^{9-}$, two aqua O atoms (O*w*), and four terminal O atoms from $[W_5O_{18}]^{6-}$. On the other hand, *Site II* consists of four bridging O atoms from $[SbW_9O_{33}]^{9-}$ and four terminal O atoms from $[W_5O_{18}]^{6-}$. This paper describes the effect of ionic size of $RE^{3+}$ on populations at *Site I* and *Site II* in $[(RE)_2(H_2O)_2(SbW_9O_{33})(W_5O_{18})_2]^{15-}$, which was studied by photoluminescence spectroscopy and X-ray crystallography in Eu/Lu- and Eu/Y-mixed system (ionic radii for eight-fold coordination:[10] $Y^{3+}$, 1.019; $Eu^{3+}$, 1.066; $Lu^{3+}$, 0.977 Å). The results provide important information for the construction of large RE-polyoxometalates. Although there are a few other examples of polynuclear complexes comprising non-equivalent RE sites,[3,11–13] the effect of $RE^{3+}$ size on the site-population selectivity has not been discussed. We also report a novel trinuclear RE complex, $[Lu_3(H_2O)_4(SbW_9O_{33})_2(W_5O_{18})_2]^{21-}$, which was prepared by a trial of the replacement of RE atoms in $[(RE)_2(H_2O)_2(SbW_9O_{33})(W_5O_{18})_2]^{15-}$ by Lu atoms.

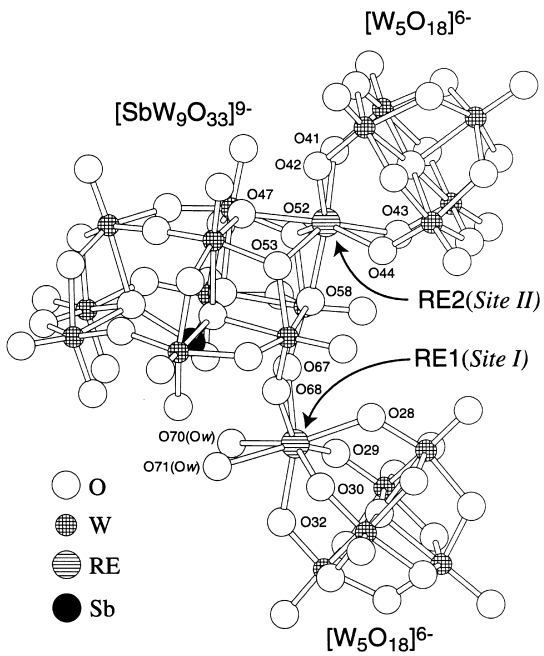


Fig. 1. View of the $[(RE)_2(H_2O)_2(SbW_9O_{33})(W_5O_{18})_2]^{15-}$ anion. Only selected atoms are labeled.

## Experimental

**$K_{15}[Eu_2(H_2O)_2(SbW_9O_{33})(W_5O_{18})_2]\cdot 22H_2O$ (1).**[14] **1** was synthesized by improving the procedure of the previous study.[9] $Sb_2O_3$ (0.13 g, 0.89 mmol Sb) and $Eu_2O_3$ (0.32 g, 1.80 mmol Eu) were dissolved in hydrochloric acid (12 mol $dm^{-3}$, 4 mL) with

heating. This solution was added dropwise to a tungstate solution (at room temperature) which had been prepared by dissolving $WO_3$ (4.0 g, 17 mmol W) and KOH (2.5 g) in hot water (60 mL). The solution pH of was kept at ca. 7 by aqueous KOH (ca. 1 mol $dm^{-3}$, 10 mL) during the addition, and finally adjusted to ca. 7. 5. The solution was heated at 80–90 °C with stirring to reduce its volume to ca. 50 mL, then cooled to room temperature. The precipitate in the reactant solution was removed by filtration and the filtrate was cooled to 5 °C for 1 d. A transparent viscous phase appeared at the bottom of the container, over which a few grains of seed-crystals were added. After 1 d, transparent crystals of **1** appeared in the viscous substance. The product was collected by filtration after 1 week, and dried in air on filter paper. Yield 1.1 g (20% based on W). Elemental analysis was performed on a X-ray fluorescence analyzer (JEOL JSX-3200). Observed K, 10; Sb, 2.2; Eu, 6.6; W, 59%. Calcd for $H_{48}O_{93}K_{15}SbEu_2W_{19}$: K, 9.71; Sb, 2.02; Eu, 5.03; W, 57.82%.

**$K_{15}[Eu_{1.27}Lu_{0.73}(H_2O)_2(SbW_9O_{33})(W_5O_{18})_2]\cdot 24H_2O$ (2).**[15] **2** was synthesized by a similar procedure using $Eu_2O_3$ (0.16 g, 0.91 mmol Eu) and $Lu_2O_3$ (0.18 g, 0.90 mmol Lu) with a Eu:Lu = 1:1 ratio. Yield 2.2 g (40% based on W). Obsd K, 9.8; Sb, 2.1; Eu 3.4; Lu, 2.2; W, 57%. Calcd for $H_{52}O_{95}K_{15}SbEu_{1.27}Lu_{0.73}W_{19}$: K, 9.62; Sb, 2.00; Eu, 3.17; Lu, 2.10; W, 57.32%.

**$K_{15}[Eu_{0.56}Lu_{1.44}(H_2O)_2(SbW_9O_{33})(W_5O_{18})_2]\cdot 20H_2O$ (3).**[15] A mixture of $Eu_2O_3$ (0.08 g, 0.45 mmol Eu) and $Lu_2O_3$ (0.15 g, 1.35 mmol Lu) with a Eu:Lu = 1:3 ratio was used for the starting material. Yield 1.9 g (36% based on W). Obsd K, 9.8; Eu 1.4; Lu, 4.2; Sb, 2.3; W, 59%. Calcd for $H_{44}O_{91}K_{15}SbEu_{0.56}Lu_{1.44}W_{19}$: K, 9.71; Eu, 1.41; Lu, 4.17; Sb, 2.02; W, 57.84%.

**$K_{15}[Eu_{0.87}Y_{1.13}(H_2O)_2(SbW_9O_{33})(W_5O_{18})_2]\cdot 20H_2O$ (4).**[14] A mixture of $Eu_2O_3$ (0.16 g, 0.90 mmol Eu) and $Y_2O_3$ (0.102 g, 0.90 mmol Y) with a Eu:Y = 1:1 ratio was used for the starting material. Yield 2.7 g (50% based on W). Obsd K, 9.6; Y, 1.8; Sb, 2.2; Eu 2.2; W, 60%. Calcd for $H_{44}O_{91}K_{15}Y_{1.13}SbEu_{0.87}W_{19}$: K, 9.88; Y, 1.69; Sb, 2.05; Eu, 2.23; W, 58.86%.

**$K_{15}[Eu_{0.41}Y_{1.59}(H_2O)_2(SbW_9O_{33})(W_5O_{18})_2]\cdot 18H_2O$ (5).**[14] A mixture of $Eu_2O_3$ (0.08 g, 0.45 mmol Eu) and $Y_2O_3$ (0.153 g, 1.35 mmol Y) with a Eu:Y = 1:3 ratio was used for the starting material. Yield 3.0 g (57% based on W). Obsd K, 9.9; Y, 2.6; Sb, 2.2; Eu 1.2; W, 62%. Calcd for $H_{40}O_{89}K_{15}Y_{1.59}SbEu_{0.41}W_{19}$: K, 9.99; Y, 2.41; Sb, 2.07; Eu, 1.06; W, 59.52%.

**$K_{15}[Eu_{0.22}Y_{1.78}(H_2O)_2(SbW_9O_{33})(W_5O_{18})_2]\cdot\sim 20H_2O$ (6).**[15] A mixture of $Eu_2O_3$ (0.04 g, 0.23 mmol Eu) and $Y_2O_3$ (0.357 g, 1.57 mmol Y) with a Eu:Y = 1:7 ratio was used for the starting material. Yield 2.7 g (51% based on W). Obsd K, 9.8; Y, 2.7; Sb, 2.1; Eu 0.57; W, 62%. Calcd for $H_{44}O_{91}K_{15}Y_{1.78}SbEu_{0.22}W_{19}$: K, 9.95; Y, 2.69; Sb, 2.07; Eu, 0.57; W, 59.27%.

**$K_{15}[Y_2(H_2O)_2(SbW_9O_{33})(W_5O_{18})_2]\cdot 23H_2O$ (7).**[14] **7** was synthesized according to the method reported previously.[9] Yield 3.8 g (72% based on W). Obsd K, 10; Y, 3.5; Sb, 1.9; W, 58%. Calcd for $H_{50}O_{94}K_{15}Y_2SbW_{19}$: K, 9.88; Y, 3.00; Sb, 2.05; W, 58.87%.

**$K_{15}[Dy_2(H_2O)_2(SbW_9O_{33})(W_5O_{18})_2]\cdot 22H_2O$ (8).**[14] **8** was synthesized using $Dy_2O_3$ (0.34 g, 1.8 mmol Dy) in a synthesis procedure similar to that of **1**. Yield 4.3 g (80% based on W). Obsd K, 10; Sb, 1.8; Dy, 6.3; W, 57%. Calcd for $H_{48}O_{93}K_{15}SbDy_2W_{19}$: K, 9.67; Sb, 2.01; Dy, 5.36; W, 57.62%.

**$K_{21}[Lu_3(H_2O)_4(SbW_9O_{33})_2(W_5O_{18})_2]\cdot 31H_2O$ (9).**[14] **9** was synthesized using $Lu_2O_3$ (0.36 g, 1.8 mmol Lu) in a synthesis procedure similar to that of **1**. Yield 2.2 g (40% based on W). Obsd K, 9.1; Lu, 5.6; Sb, 2.1; W, 57%. Calcd for $H_{70}O_{137}K_{21}Sb_2Lu_3W_{28}$: K, 9.12; Lu, 5.83; Sb, 2.71; W, 57.20%.

**IR Spectroscopy.**[16] IR spectra for **1**, **2**, and **6–9** were recorded on a Jasco FT/IR-410 spectrometer by the conventional KBr disc method (the spectra were deposited as Fig. 4S). All the absorption bands for **1**, **2**, and **6–8** were similar to those for the Sm- and Er-analogs. The spectrum for **9** is similar to those of other complexes except for a stronger absorption band at 878 $cm^{-1}$.

**X-ray Crystallography.**[17] Single crystal X-ray structural analyses were performed for compounds **1**, **3–5**, and **7–9**. The single crystals were sealed in glass capillaries and mounted on a Rigaku RAXIS-RAPID imaging plate diffractometer with monochromatized Mo $K\alpha$ radiation ($\lambda$ = 0.71069 Å). A numerical absorption correction (Numabs[18] and Shape[19]) was made. The structures were solved by SIR92[20] and refined with full-matrix least squares using all data collected. All the compounds **1**, **3**-**5**, and **7**-**8** are isostructural, containing $[(RE)_2(H_2O)_2(SbW_9O_{33})(W_5O_{18})_2]^{15-}$ anion (Fig. 1). Since Eu and Lu (or Y) atoms are disordering among *Site I* and *Site II* in complexes **3**, **4**, and **5**, the refinement was performed under the following conditions: $xyz(Eu)_{Site\ I} = xyz(Lu/Y)_{Site\ I}$ ; $xyz(Eu)_{Site\ II} = xyz(Lu/Y)_{Site\ II}$ ; $B_{iso}(Eu)_{Site\ I} = B_{iso}(Eu)_{Site\ II}$; $B_{iso}(Lu/Y)_{Site\ I} = B_{iso}(Lu/Y)_{Site\ II}$; $Occ(Eu)_{Site\ I} + Occ(Lu/Y)_{Site\ I} = 1.0$; $Occ(Eu)_{Site\ II} + Occ(Lu/Y)_{Site\ II} = 1.0$, where $xyz(RE)_{Site\ I/II}$ , $B_{iso}(RE)_{Site\ I/II}$ , and $Occ(RE)_{Site\ I/II}$ denote positional and isotropic thermal parameters, and site occupancies of RE at *Site I/II*, respectively. The crystallographic and refinement data are summarized in Table 1.

**Photoluminescence Spectra.**[16] Light at 395-nm corresponding to the $Eu^{3+}$: $^7F_0 \rightarrow {}^5L_6$ absorption was generated by a 500 W Xe-lamp and a grating monochromator (Nikon G-250) and this light was irradiated to freshly prepared samples **1–6**. The resulting luminescence was introduced to a grating monochromator (SPEX 750M) equipped with a photomultiplier (HAMAMATSU R-928) and scanned in 570–720 nm range. The output signal was processed with a lock-in amplifier (NF LI-575) and recorded. Evacuation of the samples resulted in a small change in luminescence spectra, probably because the ligand fields of $Eu^{3+}$ are slightly changed by the removal of crystallization water molecules.

## Results and Discussion

**Photoluminescence Spectroscopy of $[Eu_x(RE)_{2-x}(H_2O)_2(SbW_9O_{33})(W_5O_{18})_2]^{15-}$ (RE = Lu and Y).** Although no X-ray structural characterization for **2** nor **6** has been made, the results for the elemental analyses and IR spectra strongly support the conclusion that **2** and **6** are isostructural with **1** and **3–5**. Figure 2(a) shows room-temperature photoluminescence spectra of $K_{15}[Eu_xLu_{2-x}(H_2O)_2(SbW_9O_{33})(W_5O_{18})_2]\cdot nH_2O$ ($x$ = 2.0 (**1**), 1.27 (**2**), 0.56 (**3**)). The spectra are characteristic of the $Eu^{3+}$ f-f transition, comprising sharp lines due to $^5D_0 \rightarrow {}^7F_J$ (J = 0–4) transitions in the 580–710 nm range. The feature of the photoluminescence spectrum of $K_{15}[Eu_xLu_{2-x}(H_2O)_2(SbW_9O_{33})(W_5O_{18})_2]\cdot nH_2O$ depends on $x$, indicating that luminescence patterns of $Eu^{3+}$ at *Sites I* and *II* are different and that the ratio of $Eu^{3+}$-population at the two sites varies with the Eu:Lu ratio. Figure 3 represents high resolution spectra of the $^5D_0 \rightarrow {}^7F_J$ ($J$ = 0, 1, 2, 4) transitions. We categorized the peaks into two groups, *A* and *B*: the *A* peaks exist in all **1–3** samples, while the *B* peaks lessen their relative intensities (against *A* peaks) with a decrease of $x$. A decrease of the Eu-content in the samples from **1** ($x$ = 2.0) to **3** ($x$ = 0.56) brought about a corresponding decrease of the occupancy of $Eu^{3+}$ at either *Site I* or *II*, as shown in the spectrum of **3** where *A* peaks

Table 1. Crystal and Refinement Data for **1**, **3**–**5**, and **7**–**9**

| | **1** | **3**[a)] | **4** | **5** | **7** | **8** | **9** |
|---|---|---|---|---|---|---|---|
| Empirical formula | $H_{48}O_{93}K_{15}SbEu_2W_{19}$ | $H_{44}O_{91}K_{15}SbEu_{0.56}Lu_{1.44}W_{19}$ | $H_{44}O_{91}K_{15}Y_{1.13}SbEu_{0.87}W_{19}$ | $H_{40}O_{91}K_{15}Y_{1.59}SbEu_{0.41}W_{19}$ | $H_{50}O_{94}K_{15}Y_2SbW_{19}$ | $H_{48}O_{93}K_{15}SbDy_2W_{19}$ | $H_{70}O_{137}K_{21}Sb_2Lu_3W_{28}$ |
| Crystal size/mm$^3$ | | | | | | | |
| Formula weight /g mol$^{-1}$ | 6041.62 | 6038.54 | 5934.34 | 5901.30 | 5933.52 | 6062.70 | 8999.74 |
| Space group (number) | $P\bar{1}$ (#2) | $P\bar{1}$ (#2) | $P\bar{1}$ (#2) | $P\bar{1}$ (#2) | $P\bar{1}$ (#2) | $P\bar{1}$ (#2) | $C2/c$ (#15) |
| $a$/Å | 16.4602(6) | 16.3729(4) | 16.3173(6) | 16.3045(5) | 16.3469(8) | 16.3547(6) | 42.8834(9) |
| $b$/Å | 17.2791(8) | 17.3008(4) | 17.0375(6) | 17.0851(4) | 17.1507(7) | 17.1214(6) | 12.9859(3) |
| $c$/Å | 20.028(1) | 20.1365(5) | 20.1291(8) | 20.0636(6) | 20.177(1) | 20.0767(5) | 25.4287(6) |
| $\alpha$/deg | 76.545(1) | 76.638(1) | 76.813(1) | 76.7542(5) | 76.604(1) | 76.811(1) | |
| $\beta$/deg | 85.237(1) | 85.4876(9) | 86.142(1) | 85.8136(5) | 85.896(1) | 85.781(2) | 114.4006(9) |
| $\gamma$/deg | 63.581(2) | 63.760(1) | 64.329(1) | 64.277(1) | 64.123(1) | 64.091(1) | |
| V/Å$^3$ | 4960.0(4) | 4975.8(2) | 4907.5(3) | 4899.0(2) | 4984.2(4) | 4921.1(3) | 12895.8(5) |
| $Z$ | 2 | 2 | 2 | 2 | 2 | 2 | 4 |
| $D_{calc}$/g cm$^{-3}$ | 4.405 | 4.074 | 4.016 | 4.000 | 3.982 | 4.091 | 4.635 |
| $\mu$/mm$^{-1}$ | 24.202 | 24.560 | 24.410 | 24.433 | 24.176 | 24.642 | 28.374 |
| $R_1$ ($> 2\sigma(I)$) | 0.087 | 0.085 | 0.082 | 0.079 | 0.090 | 0.076 | 0.056 |
| $wR_2$ (all data) | 0.183 | 0.187 | 0.186 | 0.174 | 0.179 | 0.167 | 0.136 |
| GOF | 1.31 | 1.56 | 1.55 | 1.50 | 1.24 | 1.25 | 0.86 |
| No. reflns | | | | | | | |
| total | 50684 | 40810 | 31722 | 37865 | 57158 | 58086 | 69492 |
| independent | 27056 | 28214 | 22456 | 27409 | 28209 | 28123 | 18403 |
| No. parameters | 760 | 1087 | 1054 | 1081 | 1065 | 1088 | 523 |
| $T_{min}$, $T_{max}$ | 0.0503, 0.1480 | 0.0237, 0.0873 | 0.0542, 0.1495 | 0.0184, 0.1455 | 0.1101, 0.3096 | 0.0316, 0.1378 | 0.0839, 0.5979 |
| $\Delta\rho_{min}$, $\Delta\rho_{max}$/eÅ$^{-3}$ | −3.10, 3.15 | −5.11, 6.72 | −3.24, 4.87 | −3.38, 4.79 | −2.60, 4.04 | −3.41, 3.75 | −5.48, 4.44 |

a) The empirical formula for **3** is based on the elemental analysis.

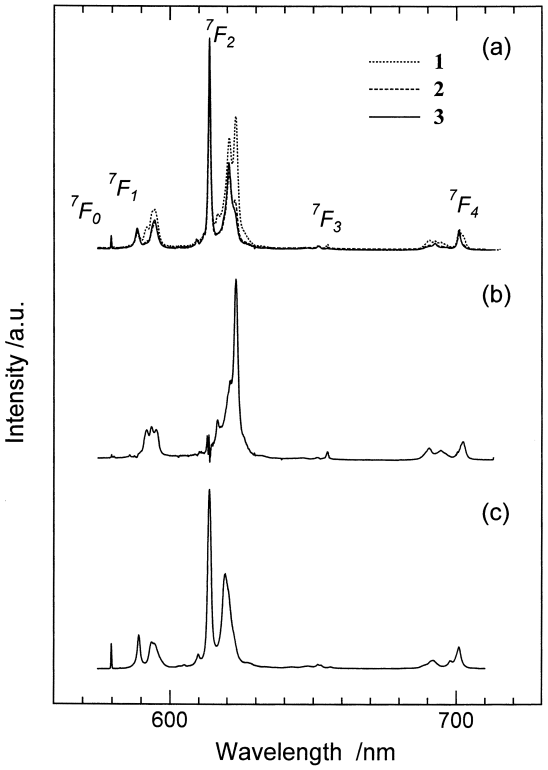


Fig. 2. Room-temperature photoluminescence spectra of $K_{15}[Eu_xLu_{2-x}(H_2O)_2(SbW_9O_{33})(W_5O_{18})_2]\cdot nH_2O$ ($x$ = 2.0 (**1**), 1.27 (**2**), and 0.56 (**3**)) (a), the difference spectrum obtained by {spectrum **1**}-$c$·{spectrum **3**} where $c$ denotes an optimized coefficient (b), and $K_{15}H_3[Eu_3(H_2O)_3(SbW_9O_{33})(W_5O_{18})_3]\cdot 25.5H_2O$[21] (c), Excitation wavelength: 395 nm.

Table 2. Eu:RE Ratios and Refined Site Occupancies (*Occ*) for the **3**–**5** Complexes

| | **3** (RE = Lu) | **4** (RE = Y) | **5** (RE = Y) |
|---|---|---|---|
| $Eu:RE_{prep}$ [a)] | 1:3 | 1:1 | 1:3 |
| $Eu:RE_{anal}$ [b)] | 0.56:1.44 | 0.82:1.18 | 0.42:1.58 |
| $Occ(Eu)_{Site\ I}$ | 0.76(2) | 0.62(1) | 0.330(9) |
| $Occ(RE)_{Site\ I}$ | 0.24 | 0.38 | 0.670 |
| $Occ(Eu)_{Site\ II}$ | 0.04(3) | 0.25(1) | 0.083(8) |
| $Occ(RE)_{Site\ II}$ | 0.96 | 0.75 | 0.917 |
| $Occ(Eu)_{Site\ I} + Occ(Eu)_{Site\ II}$ :$Occ(RE)_{Site\ I} + Occ(RE)_{Site\ II}$ | 0.80:1.20 | 0.87:1.13 | 0.41:1.59 |

a) Eu:RE ratio loaded for the synthesis.
b) analyzed Eu:RE ratio in the complexes.

are predominant. The spectrum of **3** allows us to estimate the *B* peaks-alone spectrum by subtracting the spectrum of **3** from that of **1** with an optimized coefficient $c$ (i.e. {spectrum **1**}-$c$·{spectrum **3**}), which is shown in Fig. 2(b). The significant difference in the luminescence pattern between **3** in Fig. 2(a) and Fig. 2(b) can be attributed to a difference in local symmetries of square-antiprismatic crystal field for the two RE sites (Fig. 1): an approximate local symmetry for *Site I* is $C_s$ due to two long RE1-O70, -O71 bonds, and that for *Site II* is $C_{2v}$ due two long RE2-O52, -O53 bonds.[9]

An assignment of *A* or *B* peaks to *Site I* or *II* was made based on the luminescence spectrum of $[Eu_3(H_2O)_3(SbW_9O_{33})$-

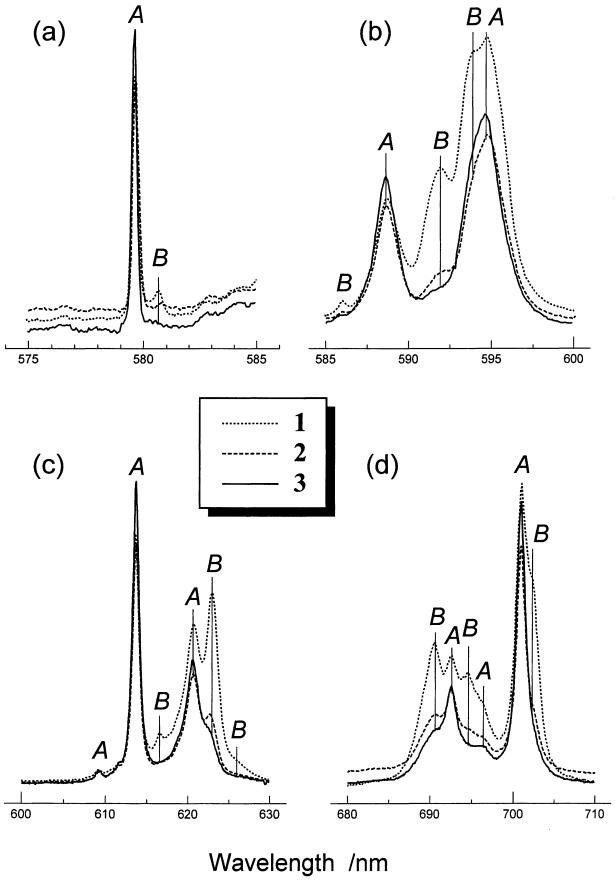


Fig. 3. High-resolution photoluminescence spectra of **1**–**3**: $^5D_0 \rightarrow {}^7F_0$ (a), $\rightarrow {}^7F_1$ (b), $\rightarrow {}^7F_2$ (c), and $\rightarrow {}^7F_4$ (d). The *B* peaks decline their relative intensities against *A* peaks with a decrease of the Eu-content from $x$ = 2.0 (**1**), 1.27 (**2**) and 0.56 (**3**).

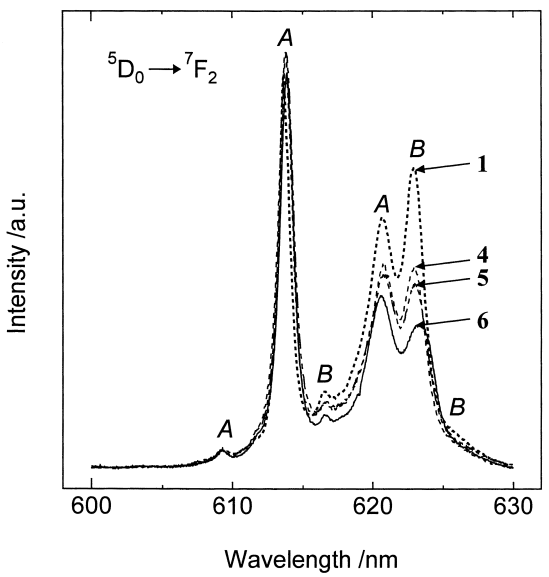


Fig. 4. High-resolution photoluminescence spectra of $^5D_0 \rightarrow {}^7F_2$ transition for **1** and **4**–**6**. The *B* peaks decline their relative intensities against *A* peaks with a decrease of the Eu-content from $x$ = 2.0 (**1**), 0.87 (**4**), 0.41 (**5**), and 0.22 (**6**).

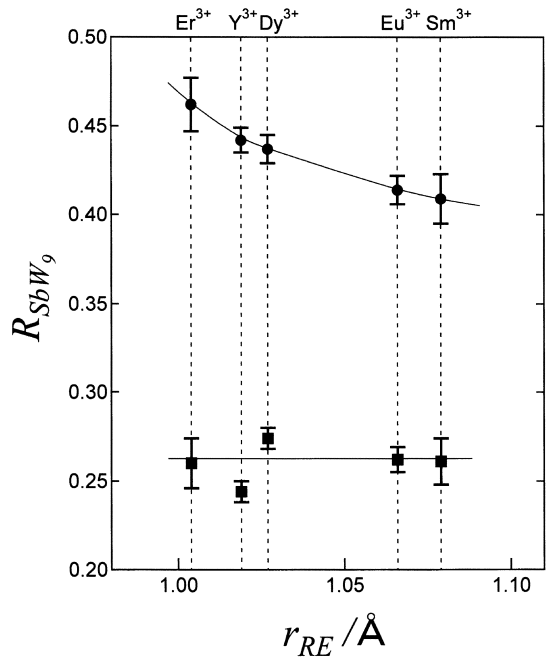


Fig. 5. Plot of $R_{SbW9}$ vs $r_{RE}$ for $[(RE)_2(H_2O)_2(SbW_9O_{33})(W_5O_{18})_2]^{15-}$ (RE = Er, Y (**7**), Dy (**8**), Eu (**1**), Sm) (see Table 3).

$(W_5O_{18})_3]^{18-}$ (Fig. 2(c)),[21] because the coordination environment of Eu in $[Eu_3(H_2O)_3(SbW_9O_{33})(W_5O_{18})_3]^{18-}$ is similar to that of *Site I*. Line profile and relative intensities of each $^5D_0 \rightarrow {}^7F_J$ transition in Fig. 2(c) are similar to those of **3** (Fig. 2(a)). Thus, the spectrum of **3** (i.e. *A* peaks) can be assigned to the emission mainly from *Site I*, alternatively *B* peaks (Fig. 2(b)) can be assigned to *Site II*.

In analogy to the Eu/Lu-system, luminescence intensities of *B* peaks for $K_{15}[Eu_xY_{2-x}(H_2O)_2(SbW_9O_{33})(W_5O_{18})_2]\cdot nH_2O$ ($x$ = 2.0 (**1**), 0.87 (**4**), 0.41 (**5**), 0.22 (**6**)) decreased with decreasing $x$. Figure 4 shows high-resolution luminescence spectrum of $^5D_0 \rightarrow {}^7F_2$ transition for **1**, and **4**–**6**.[16] It should be noted that *B* peaks remain even at the lowest Eu-concentration (i.e. $x$ = 0.22 for **6**). This indicates that RE size-selectivity of *Site II* for the Y/Eu-system is lower than that for the Eu/Lu-system, because the difference in ionic radius between $Eu^{3+}$ (1.066 Å) and $Y^{3+}$ (1.019 Å) is smaller than that between $Eu^{3+}$ and $Lu^{3+}$ (0.977 Å).

**X-ray Crystallographic Analysis of $[(RE)_2(H_2O)_2(SbW_9O_{33})(W_5O_{18})_2]^{15-}$.** In order to estimate the population of RE atoms in the two sites, occupancies of Eu, Lu, and Y at *Site I* and *II* in **3**, **4**, and **5** were also analyzed by X-ray crystallography under the conditions described in the experimental section. Table 2 summarizes values of $Occ(RE)_{Site\ I/II}$, $Eu:RE_{prep}$ (initial Eu:RE ratios loaded for the synthesis), and $Eu:RE_{anal}$ (Eu:RE ratios in the complex) for **3**–**5**. The $\{Occ(Eu)_{Site\ I} + Occ(Eu)_{Site\ II}\}:\{Occ(Y)_{Site\ I} + Occ(Y)_{Site\ II}\}$ ratios for **4** and **5** (0.87:1.13 and 0.41:1.59, respectively) are approximately consistent with the $Eu:Y_{anal}$ ratios (0.82:1.18 and 0.42:1.58, respectively), indicating that the crystallographic refinement for *Occ* is plausible. However, one may point out that a relatively large displacement of $\{Occ(Eu)_{Site\ I}+Occ(Eu)_{Site\ II}\}:\{Occ(Lu)_{Site\ I}+Occ(Lu)_{Site\ II}\}$ (= 0.80:1.20) from $Eu:Lu_{anal}$ (= 0.56:1.44) for **3**, is probably due to a small difference in

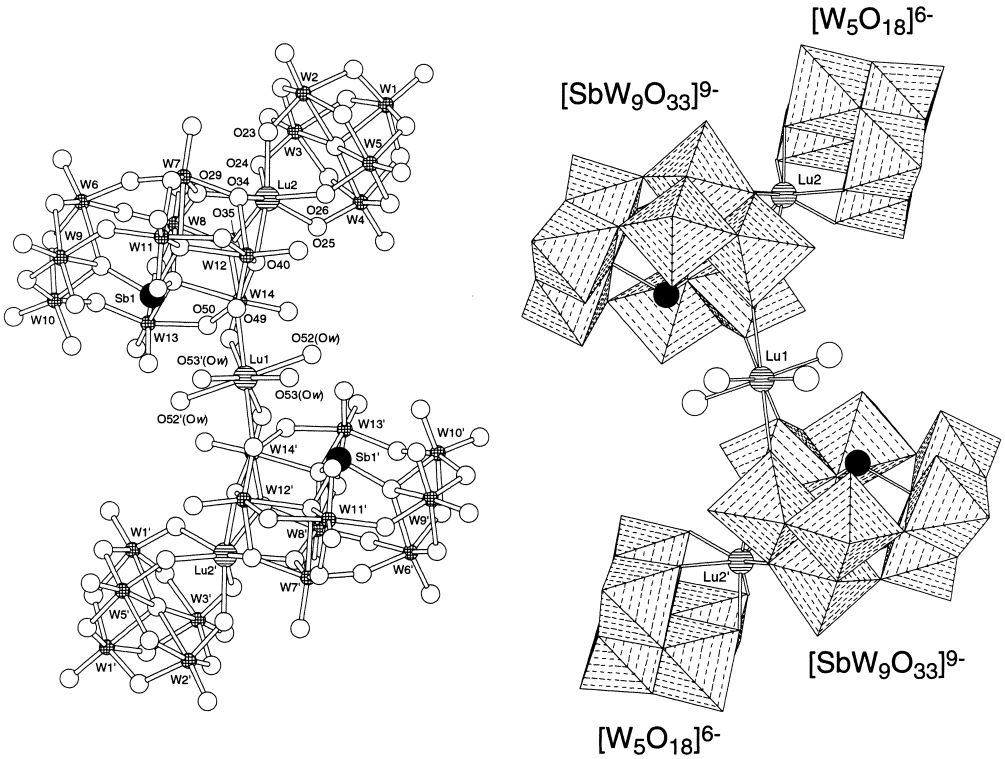


Fig. 6. Ball-and-stick (left) and polyhedral (right) models of the $[Lu_3(H_2O)_4(SbW_9O_{33})(W_5O_{18})_2]^{21-}$ anion in **9** viewed along the crystallographic $C_2$-axis. Only selected atoms are labeled.

Table 3. RE–O Distances ($d$), bond valence sums (BVS),[1)] and $R_{SbW9}$[2)] for $[(RE)_2(H_2O)_2(SbW_9O_{33})(W_5O_{18})_2]^{15-}$ (RE = Er,[3)] Y (**7**), Dy (**8**), Eu (**1**), Sm[3)]).

| | RE = Er[3)] | | | RE = Y (**7**) | | | RE = Dy (**8**) | | | RE = Eu (**1**) | | | RE = Sm[3)] | | |
|---|---|---|---|---|---|---|---|---|---|---|---|---|---|---|---|
| | $d$/Å | BVS | $R_{SbW9}$ | $d$/Å | BVS | $R_{SbW9}$ | $d$/Å | BVS[1)] | $R_{SbW9}$ | $d$/Å | BVS | $R_{SbW9}$ | $d$/Å | BVS | $R_{SbW9}$ |
| RE1 | | | | | | | | | | | | | | | |
| –O28 | 2.27(4) | | | 2.32(2) | | | 2.38(1) | | | 2.39(2) | | | 2.37(3) | | |
| –O29 | 2.29(4) | 1.87(9)[a] | | 2.32(2) | 1.76(4)[a] | | 2.38(1) | 1.60(4)[a] | | 2.37(2) | 1.77(4)[a] | | 2.39(3) | 1.72(8)[a] | |
| –O30 | 2.31(3) | | | 2.34(1) | | | 2.39(1) | | | 2.41(2) | | | 2.44(3) | | |
| –O32 | 2.31(4) | | b/(a+b+c) = 0.26(1) | 2.33(1) | | b/(a+b+c) = 0.244(6) | 2.35(1) | | b/(a+b+c) = 0.274(6) | 2.36(2) | | b/(a+b+c) = 0.262(7) | 2.42(2) | | b/(a+b+c) = 0.26(1) |
| –O67 | 2.31(3) | 0.85(5)[b] | | 2.38(1) | 0.76(2)[b] | | 2.36(1) | 0.83(2)[b] | | 2.42(1) | 0.84(3)[b] | | 2.39(2) | 0.81(5)[b] | |
| –O68 | 2.34(3) | | | 2.38(1) | | | 2.37(1) | | | 2.38(2) | | | 2.46(2) | | |
| –O70 | 2.43(3) | 0.54(4)[c] | | 2.46(1) | 0.58(2)[c] | | 2.50(1) | 0.59(2)[c] | | 2.48(2) | 0.59(2)[c] | | 2.54(2) | 0.57(3)[c] | |
| –O71 | 2.54(3) | | | 2.48(1) | | | 2.46(1) | | | 2.56(2) | | | 2.54(2) | | |
| RE2 | | | | | | | | | | | | | | | |
| –O41 | 2.30(3) | | | 2.34(1) | | | 2.34(1) | | | 2.39(1) | | | 2.45(3) | | |
| –O42 | 2.41(3) | 1.63(7)[d] | | 2.35(1) | 1.68(4)[d] | | 2.34(1) | 1.83(4)[d] | | 2.39(2) | 1.84(4)[d] | | 2.36(3) | 1.91(8)[d] | |
| –O43 | 2.31(3) | | | 2.34(2) | | | 2.35(2) | | | 2.33(2) | | | 2.31(2) | | |
| –O44 | 2.35(2) | | e/(d+e) = 0.46(2) | 2.35(1) | | e/(d+e) = 0.442(7) | 2.29(1) | | e/(d+e) = 0.437(8) | 2.37(2) | | e/(d+e) = 0.414(8) | 2.35(2) | | e/(d+e) = 0.41(1) |
| –O47 | 2.33(3) | | | 2.39(2) | | | 2.40(1) | | | 2.47(1) | | | 2.45(2) | | |
| –O52 | 2.53(3) | 1.40(6)[e] | | 2.47(1) | 1.33(3)[e] | | 2.42(1) | 1.42(2)[e] | | 2.51(1) | 1.30(3)[e] | | 2.52(2) | 1.32(5)[e] | |
| –O53 | 2.44(3) | | | 2.46(2) | | | 2.47(1) | | | 2.51(1) | | | 2.53(2) | | |
| –O58 | 2.32(3) | | | 2.38(1) | | | 2.38(1) | | | 2.45(1) | | | 2.46(3) | | |

1) Bond valence sums (BVS) for selected RE–O bonds calculated by $\Sigma\exp[(d-d_0)/B]$, where $d_0 = 2.041$ and $B = 0.335$ for Er–O, $d_0 = 2.047$ and $B = 0.340$ for Y–O, $d_0 = 2.067$ and $B = 0.335$ for Dy–O, $d_0 = 2.106$ and $B = 0.337$ for Eu–O, $d_0 = 2.118$ and $B = 0.337$ for Sm–O (see Ref. 22). The standard deviations of BVS are denoted in parentheses.
2) Ratios of BVS for RE1–O67, –O68, and RE2–O47, –O52, –O53, –O58 bonds to the total BVS of RE1 and RE2. The standard deviations of $R_{SbW9}$ are denoted in parentheses.
3) Ref. 9.

Table 4. Lu–O Distances (Å) in **9**

| | | |
|---|---|---|
| Lu1–O49 | ×2 | 2.39(1) |
| –O50 | ×2 | 2.25(1) |
| –O52 | ×2 | 2.41(1) |
| –O53 | ×2 | 2.34(2) |
| Lu2–O23 | ×1 | 2.26(1) |
| –O24 | ×1 | 2.31(1) |
| –O25 | ×1 | 2.28(1) |
| –O26 | ×1 | 2.32(1) |
| –O29 | ×1 | 2.30(1) |
| –O34 | ×1 | 2.43(1) |
| –O35 | ×1 | 2.44(1) |
| –O40 | ×1 | 2.33(1) |

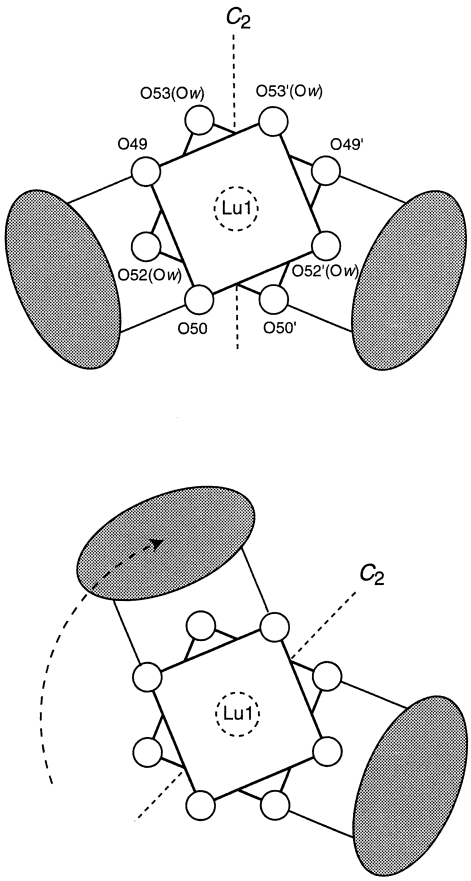


Fig. 7. Schematic drawing of the $[Lu_3(H_2O)_4(SbW_9O_{33})(W_5O_{18})_2]^{21-}$ anion in **9**. The shaded groups denote two $[Lu(2)(SbW_9O_{33})(W_5O_{18})]^{12-}$ moieties. The square-antiprismatically arranged eight O atoms around Lu1 are represented by open spheres. The original conformation (top) and the hypothetical enantiomer (bottom) formed by rotating one of the two $[Lu(2)(SbW_9O_{33})(W_5O_{18})]^{12-}$ moieties (see text).

the scattering factors between Eu (atomic number 63) and Lu (atomic number 71). For all the samples, $Occ(Eu)_{Site\ II}/Occ(RE)_{Site\ II}$ values are smaller than the $Eu:RE_{prep}$ ratios, and $Occ(Eu)_{Site\ I}/Occ(RE)_{Site\ I}$ are larger (Table 2). Also, $Occ(Eu)_{Site\ I}/Occ(Y)_{Site\ I}$ (= 1.63) is smaller than $Occ(Y)_{Site\ II}/Occ(Eu)_{Site\ II}$ (= 3.00) for sample **4** with $Eu:Y_{prep} = 1:1$. These results let us conclude that a small RE atom favorably occupied *Site II* and a large RE atom *Site I*, and that the selectivity for small RE at *Site II* is larger than that for large RE at *Site I*. These conclusions are supported by the fact that the peaks *A/B* in the $Eu^{3+}$-photoluminescence spectra for the Eu/RE-mixed samples (Figs. 3 and 4) correspond to the *Site I*/*Site II*, respectively. We also point out that $Occ(Eu)_{Site\ II}/Occ(Eu)_{Site\ I}$ (= 0.242) for **5** is larger than that (= 0.05) for **3**. This is approximately consistent with the fact that the relative intensity of peaks *B* for **5** (Fig. 4) is larger than that for **3** (Fig. 3(c)).

The effect of $RE^{3+}$ size on the RE–O bonding was studied for five isomorphous (with a space group of $P\bar{1}$) crystals of $K_{15-m}H_m[(RE)_2(H_2O)_2(SbW_9O_{33})(W_5O_{18})_2]\cdot nH_2O$ with RE = Y (**6**), Sm,[9] Eu (**1**), Dy (**7**), and Er[9] containing one kind of RE species (Table 1). Table 3 lists RE–O distances and bond valence sums (BVS)[22] for RE–O bonds. In order to evaluate the bond strengths for $RE2^{3+}\cdots[SbW_9O_{33}]^{9-}$ and $RE2^{3+}\cdots[W_5O_{18}]^{6-}$, ratios of BVS for RE1–O67, –O68 (for *Site I*) and RE2–O47, –O52, –O53, –O58 (for *Site II*) to the total BVS of RE atoms are also listed as $R_{SbW9}$ in Table 3. Figure 5 shows plots of $R_{SbW9}$ values against ionic radius ($r_{RE}$) of $RE^{3+}$. As shown in Fig. 5, the $R_{SbW9}$ value for RE2 decreases with increasing $r_{RE}$, while that for RE1 does not seem to be related to $r_{RE}$. This indicates that the RE size-selectivity of *Site I* is low compared with that of *Site II* (being consistent with the results of the luminescence spectroscopy and X-ray structural analyses for the Y/Eu- and Eu/Lu-systems), and that the large population of small RE cations at *Site II* results from stabilization of the $RE2^{3+}\cdots[SbW_9O_{33}]^{9-}$ bonding in the formation of $[(RE)_2(H_2O)_2(SbW_9O_{33})(W_5O_{18})_2]^{15-}$, as supported by the increase of yield of $K_{15-m}H_m[(RE)_2(H_2O)_2(SbW_9O_{33})(W_5O_{18})_2]\cdot nH_2O$ (RE = Y, Sm, Eu, Dy, Er, and Ho) with decreasing $r_{RE}$.[9]

**Molecular Structure of 9.** The structure of the new trinuclear complex, $[Lu_3(H_2O)_4(SbW_9O_{33})_2(W_5O_{18})_2]^{21-}$ (Fig. 6), in **9** is regarded as a dimeric species of two $[Lu(2)(SbW_9O_{33})(W_5O_{18})]^{12-}$ groups linked by a $[Lu(1)(H_2O)_4]^{3+}$ cation. The $[Lu(2)(SbW_9O_{33})(W_5O_{18})]^{12-}$ group consists of a $[SbW_9O_{33}]^{9-}$ ligand capped by a $[Lu(2)(W_5O_{18})]^{3-}$ group; this is isostructural with the $[(RE)(SbW_9O_{33})(W_5O_{18})]^{12-}$ fragment in the $[(RE)_2(H_2O)_2(SbW_9O_{33})(W_5O_{18})_2]^{15-}$ anion. The Lu–O bond lengths are summarized in Table 4, where O52 and O53 atoms are aqua-ligands (O*w*) coodinating Lu1. The distorted square-antiprismatic geometry around Lu2 is similar to that of *Site II* in $[(RE)_2(H_2O)_2(SbW_9O_{33})(W_5O_{18})_2]^{15-}$. The Lu1 atom, which is located on the crystallographic $C_2$ axis, achieves square-antiprismatic eight-fold coordination by four O atoms [of O49, O50, and their symmetry-related atoms] which form vacancies of the two $[SbW_9O_{33}]^{9-}$ ligands, and four aqua-ligands (O*w*) [of O52, O53, and their symmetry-related atoms]. The coordination geometry around Lu1 is schematically represented in Fig. 7. It is noteworthy that $C_2$-symmetric $[Lu_3(H_2O)_4(SbW_9O_{33})_2(W_5O_{18})_2]^{21-}$ is chiral and a rotation of one of the two $[Lu(2)(SbW_9O_{33})(W_5O_{18})]^{12-}$ groups around $S_8$ axis of the $Lu(1)O_8$ square-antiprism by about 90° produces its enantiomer (Fig. 7). The crystal of **9** contains both enantiomers with equimolar ratio because of the symmetries (centers of symmetry and glide planes) of the space group *C*2/*c*.

It is also of interest to recall that coexistence of a small portion of Eu ($Eu:Lu = 1:3$) resulted in formation of the dinucle-

ar $[Eu_{0.56}Lu_{1.44}(H_2O)_2(SbW_9O_{33})(W_5O_{18})_2]^{15-}$ (i.e. compound **3**). This indicates that a structural transformation between dinuclear and trinuclear complexes is strongly controlled by the $RE^{3+}$ species.

## Conclusion

The effect of the RE species (i.e. ionic radii) on the population in $[(RE)_2(H_2O)_2(SbW_9O_{33})(W_5O_{18})_2]^{15-}$ have been explored by $Eu^{3+}$-luminescence spectroscopy and X-ray crystallography. The results indicated that small RE favorably occupied *Site II* in the $[(RE)_2(H_2O)_2(SbW_9O_{33})(W_5O_{18})_2]^{15-}$ anion, due to a stronger RE–O bonding of $[SbW_9O_{33}]^{9-}$ bridging O atoms with small $RE^{3+}$ at *Site II*. In the mixed-RE system, the larger the difference in ionic radii, the higher the size-selectivity at *Site II*. A novel trinuclear complex, $[Lu_3(H_2O)_4(SbW_9O_{33})_2(W_5O_{18})_2]^{21-}$, was formed by a use of $Lu^{3+}$ (the smallest of the RE's) under the synthesis procedure of $[(RE)_2(H_2O)_2(SbW_9O_{33})(W_5O_{18})_2]^{15-}$. Capping of the $[(RE)(W_5O_{18})]^{3-}$ group on $[SbW_9O_{33}]^{9-}$ is common for both anions.

This work was supported in part by Grants-in-Aid for Scientific Research (No. 10304055 and 1274036) from the Ministry of Education, Culture, Sports, Science, and Technology.

## References

1 T. Yamase and H. Naruke, *Coord. Chem. Rev.*, **111**, 83 (1991).

2 H. Naruke and T. Yamase, *Bull. Chem. Soc. Jpn.*, **73**, 375 (2000).

3 K. Wassermann, M. H. Dickmann, and M. T. Pope, *Angew. Chem., Int. Ed. Engl.*, **36**, 1445 (1997).

4 T. Yamase, T. Kobayashi, M. Sugeta, and H. Naruke, *J. Phys. Chem. A*, **101**, 5046 (1997).

5 T. Yamase and H. Naruke, *J. Phys. Chem. B*, **103**, 8850 (1999).

6 R. Shiozaki, H. Goto, and Y. Kera, *Bull. Chem. Soc. Jpn.*, **66**, 2790 (1993).

7 R. Shiozaki, A. Inagaki, A. Ozaki, H. Kominami, S. Yamaguchi, J. Ichihara, and Y. Kera, *J. Alloys Compd.*, **261**, 132 (1997).

8 R. Shiozaki, A. Inagaki, H. Kominami, S. Yamaguchi, J. Ichihara, and Y. Kera, *J. Mol. Catal.*, **124**, 29 (1997).

9 H. Naruke and T. Yamase, *Bull. Chem. Soc. Jpn.*, **74**, 1289 (2001).

10 R. D. Shannon, *Acta Crystallogr., Sect. A*, **32**, 751 (1976).

11 M. Sugeta and T. Yamase, *Acta Crystallogr., Sect. C*, **53**, 1166 (1997).

12 M. T. Pope, X. Wei, K. Wassermann, M. H. Dickman, *C. R. Acad. Sci. Paris, Ser II*, **1998**, 297.

13 K. Wassermann and M. T. Pope, *Inorg. Chem.*, **40**, 2763 (2001).

14 The formula is based on the X-ray crystallography.

15 The formula is based on the elemental analysis because its accuracy is higher than that of X-ray crystallographic analysis (see text).

16 Complete photoluminescence spectra of **4**–**6** and IR spectra of **1**, **2**, and **7**–**9**, have been deposited (photoluminescence spectra: Figs. 1S–3S; IR spectra: Fig. 4S) as Document No. 75026 at the office of the Editor of Bull. Chem. Soc. Jpn.

17 The atomic coordinates, anisotropic displacement parameters, selected bond distances and angles, and ORTEP drawing are deposited (Tables 1S–14S and Fig. 5S) as Document No. 75027 at the office of the Editor of Bull. Chem. Soc. Jpn. Details of the crystal structure data can be ordered from FACHINFORMATIONSZENTRUM KARLSRUHE, 76344 EggensteinLeopoldshafen (http://www.fiz-karlsruhe.de), under the depository numbers CSD-412343 (**1**), -412344 (**3**), -412345 (**4**), -412346 (**5**), -412347 (**7**), -412348 (**8**), and -412349 (**9**).

18 T. Higashi, "Numabs — Numerical Absorption Correction," Rigaku Corporation, Tokyo (1999).

19 T. Higashi, "Shape — Program to obtain Crystal Shape using CCD camera," Rigaku Corporation, Tokyo (1999).

20 A. Altomare, M. C. Burla, M. Camalli, M. Cascarano, C. Giacovazzo, A. Guagliardi, and G. Polidori, *J. Appl. Crystallogr.*, **27**, 435 (1994).

21 T. Yamase, H. Naruke, and Y. Sasaki, *J. Chem. Soc., Dalton Trans.*, **1990**, 1687.

22 I. D. Brown, "Structure and Bonding in Crystals," ed by M. O′Keeffe and A. Navrotsky, Academic Press, New York, U.S.A. (1980), Vol. II, pp. 1–30.